Vol. 692: 23–42, 2022
https://doi.org/10.3354/meps14077

MARINE ECOLOGY PROGRESS SERIES
Mar Ecol Prog Ser

Published June 30

Zooplankton trophic structure and ecosystem productivity

Moira Décima*

Scripps Institution of Oceanography, University of California San Diego, 9500 Gilman Dr., La Jolla, CA 92093, USA

ABSTRACT: The number of trophic steps within a plankton food web plays an important role in determining the energy available to support higher-level consumers by affecting trophic transfer efficiency (TE): fewer steps can enhance TE by decreasing respiration and predation losses. In this study, trophic structure within the zooplankton community was investigated using stable isotopes in size-fractionated mesozooplankton, and related to 2 biomass proxies related to TE: the normalized biomass size spectra (NBSS) and the ratio of zooplankton:phytoplankton biomass (log_{10} (zoo:phyto)). Four regions were compared: the California Current Ecosystem (CCE — most productive), the Equatorial Pacific (EqP), the Costa Rica Dome (CRD) and the North Pacific Subtropical Gyre (NPSG — least productive). Compound-specific isotope analysis of amino acids confirmed large differences (~3‰) in the isotopic baseline among ecosystems. EqP and NPSG had low and distinct source $\delta^{15}N$ values, while CRD/CCE had high and overlapping values. Trophic differences indicated that the CCE had the lowest number (0) of trophic differences within the 4 zooplankton size classes; NPSG and EqP had the highest number (3), and CRD was intermediate (1). NBSS slopes confirmed the CCE and NPSG as extremes and statistically different from each other. TE patterns estimated from log_{10}(zoo:phyto) suggested EqP was the least efficient, while the other 3 ecosystems (despite large ranges in zooplankton and phytoplankton biomass) had similar TEs. The inverse relationship between food chain length and system productivity, a paradigm originally formulated for microbial food webs, holds for the mesozooplankton assemblage at the productivity extremes.

KEY WORDS: Nitrogen · Isotopes · Food webs · Trophic transfer efficiency · Trophic level · Trophic position · Compound-specific isotope analysis

1. INTRODUCTION

The mean number of trophic steps within a food web is a fundamental ecological characteristic linked to resource availability (primary production, PP) and trophic transfer efficiency (TE) (Kaunzinger & Morin 1998, Ward & McCann 2017). In pelagic marine systems in particular, oligotrophic systems are thought to have longer food chains compared to productive environments, because the small size of dominant phytoplankton requires intermediate steps through protistan consumers to connect to mesozooplankton (Legendre & Rassoulzadegan 1995). In the microbial food web, small nanoflagellates directly consume picophytoplankton, which are in turn consumed by larger protists, adding 1–3 steps between autotrophs and mesozooplankton (Calbet & Landry 1999), substantially decreasing energy transfer to higher levels (Landry & Calbet 2004). In contrast, food-web configurations from productive upwelling environments can more closely resemble the 'classical food chain', in which herbivorous mesozooplankton consume large phytoplankton directly, enhancing the efficiency of trophic transfer (Ryther 1969). While the paradigm that classifies food webs across a continuum from herbivorous to microbial configurations emphasizes the trophic steps in protistan and microbial pathways to metazoan zooplankton (Legendre &

*Corresponding author: mdecima@ucsd.edu

Publisher: Inter-Research · www.int-res.com

Rassoulzadegan 1995, Legendre & Rivkin 2008), similar principles apply to the number of trophic steps within the metazoan zooplankton community. In broad terms, we can think of productive upwelling ecosystems like the California Current Ecosystem (CCE) characterized by seasonal blooms of large diatoms (Venrick 2012) as primarily herbivorous during these times, as they are often accompanied by significant biomass of large herbivorous-omnivorous copepods and euphausiids (Brinton & Townsend 2003, Lavaniegos et al. 2015). In contrast, resident copepods (zooplankton) in oligotrophic environments such as the North Pacific Subtropical Gyre (NPSG) tend to feed at higher trophic levels (TLs) (Hayward 1980), and contain higher relative proportions of predatory zooplankton taxa (McGowan & Walker 1979, Landry et al. 2001). Because additional trophic steps result in considerable losses due to respiration (Ikeda 1985) and other mortality sources (Ryther 1969), longer plankton chains limit zooplankton biomass availability for higher TLs, like fish and whales.

TE, the relative amount of production transferred up the food web, is given by the ratio Production TL_{n+1}:Production TL_n, and is nominally thought to be 0.1, or 10% per TL (Ryther 1969). However, more recent studies have indicated higher variability in TE, and more surprisingly, higher TE in open-ocean oligotrophic systems (with supposed longer food chains) compared to coastal upwelling systems (San Martin et al. 2006, Irigoien et al. 2014). TE estimates can also vary according to latitude — Maureaud et al. (2017) found TEs of 13, 10 and 7% corresponding to polar, temperate and tropical systems, respectively. Model results suggest that TE specifically for zooplankton can vary between 1 and 20%, depending on temperature and phytoplankton biomass (Stock & Dunne 2010). TE is not simply set by the magnitude of PP, or the size structure of phytoplankton, as some ecosystems have low production and small phytoplankton yet high production of higher-level consumers (Bradford-Grieve et al. 2003, Marcolin et al. 2013). The extent to which TE is influenced by the number of trophic steps, the efficiency of phytoplankton entering the food web (as opposed to direct export), and metabolic efficiency in transforming biomass into production is unknown and variable among ecosystems.

In general, TE for the lower food web is hard to estimate because production of zooplankton is difficult to measure and occurs on different time scales to that of phytoplankton. Proxies for TE such as the average TL of zooplankton (Fry & Quinones 1994, Hannides et al. 2013, Armengol et al. 2019) or the $\log_{10}$ ratio of zooplankton biomass to phytoplankton biomass ($\log_{10}$(zoo:phyto)) (García-Comas et al. 2016) have been estimated in some environments. However, the TL change with increasing zooplankton size is not always addressed, although some estimates for differences between meso- and macrozooplankton have been estimated (Hunt et al. 2015, 2021, Mompean et al. 2016). Importantly, estimates of the number of trophic steps as a function of system productivity has (to the best of my knowledge) not been assessed. The relationship of TE to productivity regimes in the ocean is key because these are changing due to warming and increased stratification (Roxy et al. 2016), although patterns for upwelling systems might be different (Rykaczewski & Dunne 2010). Some modeling exercises using future scenarios of global change predict important decreases in TEs for coastal waters in particular (du Pontavice et al. 2020). Understanding how the number of trophic steps depends on production and other water column parameters (e.g. temperature, nutrients, mixed layer depth [MLD]), and affect TE is essential to predicting how changes at the base of the food web will propagate to higher TLs.

In this study, trophic structure of the crustacean-dominated zooplankton community was investigated using stable isotopes, and TE was assessed using both the normalized biomass size spectra (NBSS) and the $\log_{10}$(zoo:phyto) in four distinct areas of the North Pacific. These regions are characterized by different baseline isotopic values, nutrient limitations, primary production and phytoplankton size spectra and taxonomic composition, as well as zooplankton size and community composition.

Stable isotopes ($\delta^{13}C$ and $\delta^{15}N$) can differentiate food sources ($\delta^{13}C$ changes very little between predator and prey) from trophic interactions ($\delta^{15}N$ increases from prey to consumer) (DeNiro & Epstein 1981, Vander Zanden & Rasmussen 2001, Post 2002). The increase in $\delta^{15}N$ with each trophic step is negligible in the processing of $\delta^{13}C$ (~0.5‰), but can vary between 2 and 4‰ for $\delta^{15}N$, and a value of 3.4 ± 1‰ is typically assumed (Post 2002). Bulk tissue measurements are relatively straightforward and economical, such that many samples can be analyzed. However, variations in the baseline (relating to N source or utilization) cannot be distinguished a priori from trophic variation. This limitation can be circumvented by normalizing to either particulate organic matter or the smallest-size zooplankton. Fig. 1 depicts the 2 theoretical extreme examples of plankton food webs: a highly productive system with direct flow from phytoplankton to zooplankton, and an oligotrophic system with a size-structured food web, along with

the expected bulk $\delta^{15}N$ changes. Real plankton food webs — in which each size class consists of a mix of animals that feed at a range of TLs, small predatory copepods co-exist with large herbivorous zooplankton, and no taxon is purely herbivorous — fall somewhere between these 2 theoretical extremes. Compound-specific isotope analysis (CSIA) of amino acids (AAs) complements the traditional bulk method by differentiating baseline values from trophic processes via the selective $\delta^{15}N$ increase of certain AAs ('source' AAs retain baseline values; trophic AAs are enriched in 15N with each trophic step) (Chikaraishi et al. 2009, Hannides et al. 2009). However, CSIA-AA is limited by time-intensive analyses and cost, such that only a subset of samples is typically analyzed.

Patterns in NBSS, specifically the slope of the linear fit (Fry & Quinones 1994, Hunt et al. 2015, Mompean et al. 2016, Kerr & Dickie 2001) can be interpreted as indicative of TE (Zhou 2006). Typically, steeper slopes are associated with lower TEs (Rykaczewski & Checkley 2008, Marcolin et al. 2013, Rykaczewski 2019), although contrasting patterns have also been observed (Zhou et al. 2009, Marcolin et al. 2013). TE can also be evaluated using both zooplankton biomass as a function of phytoplankton biomass and the proxy $\log_{10}$(zoo:phyto), which has been shown to co-vary linearly with TE (García-Comas et al. 2016).

Four regions of the North Pacific — the Costa Rica Dome (CRD), the CCE, the Equatorial Pacific (EqP), and the NPSG (Fig. 2) — are compared to address the following questions: (1) What are the interregional differences in $\delta^{15}N$ and $\delta^{13}C$ isotopic baselines for these 4 contrasting ecosystems? (2) Does the relationship between zooplankton trophic structure and productivity follow the paradigm originally formulated for protistan consumers? (3) What do conclusions from isotope-based trophic structure, NBSS, and zooplankton biomass indicate about the drivers of TE in these diverse ecosystems?

2. MATERIALS AND METHODS

2.1. Oceanographic and zooplankton sampling

Zooplankton depth of collection varied slightly among systems, but in all cases included the euphotic zone to 0.1% surface irradiance penetration (CRD, EqP, NPSG = 150 m; CCE = 210 m), sampled using either a 1 m ring net (CRD, EqP, NPSG) or paired 0.71 m Bongo nets (CCE) with 202 µm mesh and

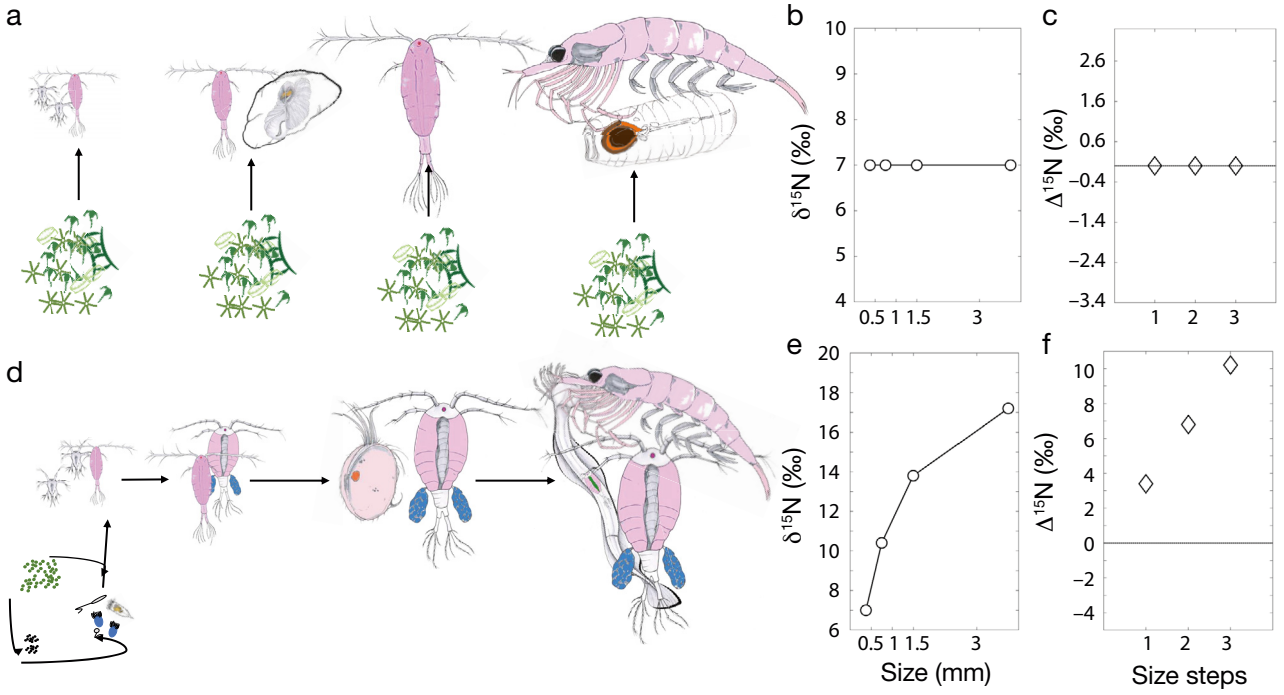

Fig. 1. Schematic of 2 idealized plankton food webs. (a–c) Not size-structured food web: (a) all zooplankton sizes feed directly on phytoplankton; (b) expected $\delta^{15}N$ of each size class when all zooplankton sizes consume phytoplankton with the same $\delta^{15}N$ at the base of the food web; (c) expected difference between each size class and the smallest (0.2–0.5 mm) zooplankton. (d–f) Size-structured food web: (d) each zooplankton size class feeds on smaller zooplankton and only the 0.2–0.5 mm zooplankton feed on phytoplankton and microzooplankton at the base of the food web; (e) expected $\delta^{15}N$ of each size class; (f) expected difference between each size class and the smallest (0.2–0.5 mm) zooplankton. Trophic enrichment of 3.4‰ per trophic step is assumed

equipped with a General Oceanics (GO) flow meter. Day/night pairs of samples were typically taken during 10:00–12:00 and 22:00–00:00 h in each ecosystem. Aliquots for zooplankton biomass were size-fractionated promptly after collection into 5 size classes (0.2–0.5, 0.5–1, 1–2, 2–5 and >5 mm) using nested sieves (Décima et al. 2016), and frozen at −80°C for later biomass and isotope analyses. Water column properties were measured daily through a conductivity-temperature-depth (CTD) rosette cast down to 200 m, and water was collected using Niskin bottles on the rosette, for chlorophyll and phytoplankton community composition.

The CRD was investigated from 22 June to 25 July 2010 in the area of 7.5–10.2° N, 87–93° W in the Eastern Tropical Pacific (Fig. 2) on the RV 'Melville'. Semi-Lagrangian experiments, called 'cycles' (denoted as C1–C4), were conducted by following a water parcel, marked by satellite-tracked drogued drifters, for a duration of 4–5 d (Landry et al. 2016). C1 was conducted in coastal waters, C2 was carried out in the central core area of the CRD, C3 was located at the periphery of the dome to the northwest and C4 was conducted within the dome, downstream from C2 (Fig. 2). Samples for isotopes were taken from each cycle (1 day/night pair). Samples for NBSS and $\log_{10}$(zoo:phyto) were day/night averages from all zooplankton tows from the 4 cycles, and PP for regional averages are from C2–C4, as no measurements were done in C1. Data for temperature and salinity presented in this manuscript were averaged from 46 casts taken at the 4 experimental locations. Zooplankton and phytoplankton biomass has been previously published (Décima et al. 2016, Landry et al. 2016, Taylor et al. 2016)

The CCE has been studied since the 1950s through the California Cooperative Oceanic Fisheries Investigations (CalCOFI) monitoring system, and more recently through the addition of the CCE to the Long-Term Ecological Research (LTER) program as a pelagic ecosystem study site. Samples from 3 CCE LTER process cruises conducted in coastal waters in the springtime were used for this study: P0605 (10 May–5 June 2006, R/V 'Knorr' — biomass and isotopes), P0704 (3–20 April 2007, R/V 'Thompson' — biomass and isotopes) and P1106 (18 June–17 July 2011, R/V 'Melville' — isotopes only). Mesozooplankton were collected following standard CalCOFI protocol (www.calcofi.org). Samples for isotopes collected on P0605 were all daytime samples, for P0704 were 1 daytime and 3 nighttime samples and P1106 samples were collected in the morning. General cruise overviews (http://cce.lternet.edu/data/cruises) and data (https://oceaninformatics.ucsd.edu) are available online. Samples used for NBSS and $\log_{10}$ (zoo:phyto) were from day/night averaged zooplankton biomass from nearshore cycles from P0704 (1 and 4) and P0605 (1, 3 and 4), and these same locations were used for regional averages of PP. CTD casts conducted on the specific experimental cycles sampled for zooplankton were averaged for regional temperature/salinity profiles: 14 casts for P0605, 9 casts for P0704 and 8 casts for P1106.

The EqP was sampled during the 2 Equatorial Biocomplexity cruises undertaken in 2004 (December, EB04) and 2005 (September, EB05) aboard the R/V 'Roger Revelle'. These cruises sampled zonal and meridional transects around the equator in the vicinity of 110–140° W. For this study, mesozooplankton bulk isotopes from 3 stations for EB04 (paired day/night) and 2 stations for EB05 (paired day/night) were used (Fig. 2). Biomass from all stations was used for NBSS and $\log_{10}$(zoo:phyto), and PP and CTDs from all stations were used for regional averages. Zooplankton biomass, phytoplankton composition and CTD data have been previously published (Décima et al. 2011, Landry et al. 2011, Taylor et al. 2011).

For sampling the NPSG, the Hawaiian Ocean Time-series (HOT) was used. Sn ALOHA (2° 45′ N, 158° 00′ W) has been sampled monthly as part of HOT since 1994 (Landry et al. 2001). Mesozooplankton are sampled at night and day over 3 days each month (weather permitting), with phytoplankton and physical conditions

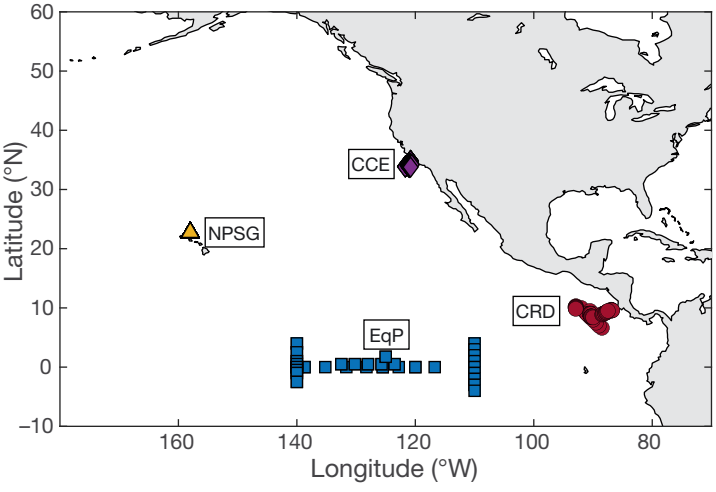

Fig. 2. Focus regions: Costa Rica Dome (CRD, red circles), California Current Ecosystem (CCE, purple diamonds), Equatorial Pacific (EqP, blue squares) and the North Pacific Subtropical Gyre (NPSG, yellow triangle). Markers: distinct sampling locations

also sampled routinely. Zooplankton samples for isotope assessment in this study came from HOT cruises 204 (August 2008), 224 (August 2010) and 235 (September 2011), and were processed using the same protocol as the other locations. Zooplankton day/night size-fractionated biomass from summer (August–September) cruises from 2005 to 2014 were used for NBSS (n = 32), CTD data from these same cruises was averaged for water column properties, and PP from these 10 cruises were averaged for a regional estimate. Zooplankton biomass, CTD and phytoplankton composition data are available online (https://hahana.soest.hawaii.edu/hot/hot_jgofs.html).

2.2. Biomass and bulk stable isotopes

Frozen samples were dried at 60°C for a minimum of 24 h. Samples were removed from the oven and weighed to 0.01 mg precision at room temperature on a Denver analytical microbalance. Biomass estimates were obtained by subtracting the initial filter weight from each final filter + biomass estimate. Integrated estimates to each sampling depth were calculated to obtain areal standing stock estimates. Once weighed, samples were homogenized with a tissue grinder in a glass test tube for bulk stable isotope analyses. Isotope analyses were only conducted on 4 of the 5 size classes, as the largest (>5 mm) did not provide quantitative samples and, depending on the system, lacked enough material to obtain sufficient material. Representative aliquots of each size class (0.2–0.5, 0.5–1, 1–2 and 2–5 mm) were weighed (0.5–1 mg per size) and packed into individual tin cups for analysis. All bulk isotope determinations were conducted at the Isotope Biogeochemistry lab at Scripps Institution of Oceanography. Isotope samples were not acidified, nor was lipid extracted prior to analyses. Acidification was not done because there were relatively few carbonate-containing organisms in the zooplankton tows (Décima et al. 2016), and acidification has been shown to artificially decrease both $\delta^{13}C$ and $\delta^{15}N$ values (Jacob et al. 2005). Values are reported for N relative to atmospheric N_2, and relative to Peedee belemnite standard for C. Data is listed in Tables S1–S4 in the Supplement at www.int-res.com/articles/suppl/m692p023_supp.pdf.

2.3. CSIA-AA

Size-fractionated zooplankton from 1 day tow and 1 night tow per region were used for CSIA-AA, using a subset of the samples analyzed for bulk isotopes. CRD had 1 day tow and 1 night tow from the dome cycles, CCE had the 2 tows from P1106, EqP had a day/night pair of tows from EB05 (Stn 22) and NPSG had the paired tow from cruise 204. Preparation followed previously described procedures (Hannides et al. 2009, Décima et al. 2013) involving 3 major steps: acid hydrolysis of the AAs, esterification of the terminal carboxyl groups and trifluoroacetylation of the amine groups (Macko et al. 1997). Sequanal grade 6 N HCl was used to hydrolyze each sample (1000–2000 µg DW). Vials were flushed with N_2, capped with a Teflon-lined cap and heated at 150°C for 70 min. Tryptophan and cysteine are destroyed during hydrolysis, and the process also converts asparagine and glutamine to aspartic acid (Asp) and glutamic acid (Glu), respectively. The hydrolysate was evaporated under N_2 at 55°C, redissolved in 1 ml 0.01 N HCl, purified by filtration (0.45 µm hydrophilic filter) and washed with 1 ml of 0.01 N HCl. The hydrolysate was further purified using cation-exchange chromatography with a 5 cm column of resin (Dowex 50WX8-400) prepared in a glass Pasteur pipette (Metges et al. 1996). AAs were eluted with NH_4OH (4 ml of 2 N) and evaporated under a stream of N_2 at 80°C to dryness. Samples were then reacidified with HCl (0.5 ml of 0.2 N), flushed with N_2, heated to 110°C for 5 min and evaporated under N_2 at 55°C to dryness. Hydrolyzed samples were esterified with 2 ml of 4:1 isopropanol:acetyl chloride, flushed with N_2 and heated to 110°C for 60 min. Samples were acylated after drying at 60°C under N_2 by adding 1 ml of 3:1 methylene chloride:trifluoracetic anhydride (TFAA) and heated for 15 min at 100°C. Purification of derivatized AAs was done by solvent extraction following Ueda et al. (1989). The acylated AA esters were evaporated at room temperature under N_2 and redissolved in 3 ml of 1:2 chloroform:P-buffer (KH_2PO_4 + Na_2HPO_4 in Milli-Q water, pH 7). The derivitized AAs were vigorous shacked within the solution, such that it partitioned into chloroform and the contaminants remained in the P-buffer. Centrifugation (10 min at 600 × *g*) separated the 2 solvents, and the chloroform was transferred to a clean vial. The solvent extraction process was then repeated. The acylation step was repeated once more to ensure derivitazation. Samples were stored at −20°C in 3:1 methylene chloride:TFAA for up to 6 mo until isotope analysis.

TFAA derivatives of AAs were analyzed by isotope ratio monitoring gas chromatography–mass spectrometry using a Delta V Plus mass spectrometer interfaced with a Trace GC gas chromatograph through a

GC-C III combustion furnace (980°C), reduction furnace (650°C) and liquid nitrogen cold trap. The samples (1 to 2 µl) were injected (split/splitless injector, 10:1 split ratio) onto a *forte* BPx5 capillary column (30 m × 0.32 mm × 1.0 µm film thickness) at an injector temperature of 180°C with a constant helium flow rate of 1.4 ml min^{-1}. The column was initially held at 50°C for 2 min and then increased to 190°C at a rate of 8°C min^{-1}. Once at 190°C, the temperature was increased at a rate of 10°C min^{-1} to 300°C, where it was held for 7.5 min. Internal reference compounds, aminoadipic acid and norleucine of known nitrogen isotopic composition were co-injected with samples and used to normalize the measured $\delta^{15}N$ values of unknown AAs. Samples were injected 3 times into the GC-C, and data are reported as mean ± SD of the 3 replicate injections.

Measurements of phenylalanine (Phe) $\delta^{15}N$ had multiple issues in these samples related to high baseline variability or co-elution with unknown peaks. Thus, $\delta^{15}N$ of Phe was not used in this study. Baseline variability was investigated using an average of 3 source AAs: lysine (Lys), glycine (Gly) and serine (Ser). The averaged trophic AAs to estimate broad trophic position (TP) were Asp, alanine (Ala) and Glu. Data is listed in Tables S5 & S6.

2.4. TPs, NBSS, $\log_{10}$(zoo:phyto) and data analyses

The CSIA-AA TP was calculated using average source and trophic values following Hannides et al. (2009). As such, differentiating between trophic pathways that involve only metazoans, using Phe and Glu $\delta^{15}N$, and those that also include protozoans, using Phe and Ala, was not possible (Décima et al. 2017, Landry & Décima 2017, Décima & Landry 2020). Average TPs were calculated using the average of 3 source AAs ($\delta^{15}N_{source}$) (Lys, Ser and Gly) and the average of 3 trophic AAs ($\delta^{15}N_{trophic}$) (Asp, Ala and Glu) (Table S1). An average trophic enrichment factor (TEF) of 7‰ was used in the calculation (Hannides et al. 2009):

$$TP_{AA} = (\delta^{15}N_{trophic} - \delta^{15}N_{source})/7 + 1 \quad (1)$$

TPs based on bulk values (TP_{bulk}) were not used to investigate trophic differences because the variability in the trophic discrimination factor (TDF) among different size classes and systems is unknown. The addition of this factor is also unnecessary to answer the question of relative differences, which relies on the variability in isotope data alone. However, TP_{bulk} was calculated using a TDF of 3.4‰ (Post 2002) to compare to CSIA values, illustrating the effect of TDF on absolute TP values, and providing a method comparison.

To investigate trophic structure within the zooplankton size fractions, differences in bulk isotopic values were examined relative to the smallest zooplankton size class (consisting of organisms 0.2–0.5 mm), denoted as $\delta^{15}N_0$:

$$\Delta^{15}N = \delta^{15}N_i - \delta^{15}N_0, \text{ for } i = 1, 2, 3 \quad (2)$$

where $\delta^{15}N_i$ refers to the isotopic values of the i^{th} size step (with size step 1 corresponding to 0.5–1 mm, size step 2 corresponding to 1–2 mm and size step 3 corresponding to 2–5 mm) (see Fig. 1b,c,e,f for an example of how the steps and change in bulk $\delta^{15}N$ are related). Size classes were defined to have trophic steps if their $\Delta^{15}N$ values were significantly different from zero and/or different to other size classes. Both C and N isotopes were investigated to understand the trophic differences in zooplankton size classes collected in the field. Violin plots were constructed using the kernel density function. Statistical comparisons were done using the non-parametric sign and Kruskal-Wallis test.

NBSS were calculated using all 5 size classes following the approach of Rykaczewski & Checkley (2008), who used size-fractionated zooplankton biomass for NBSS. Log(biomass/Δx), where biomass represents the biomass in a size fraction (mg m^{-2}) and Δx corresponds to the size interval for each size fraction (303, 495, 1000, 3000 and 5000 µm), was plotted against Log(x), where x corresponds to each size (202, 505, 1000, 2000 and 5000 µm). Spectral slopes (*m*) were calculated by fitting least-squares regression to the following:

$$\text{Log(biomass}/\Delta x) = m\,(\text{Log}(x)) + b \quad (3)$$

The difference among ecosystems was evaluated by conducting an ANCOVA, which tested the difference among the day/night average NBSS slope ($p < 0.05$).

Finally, $\log_{10}$(zoo:phyto) was calculated by vertically integrating phytoplankton carbon biomass using the trapezoidal method, and converting zooplankton dry weight to carbon using a 0.36 conversion factor (Landry et al. 2001). All plotting and statistical tests were conducted using Matlab 2021b.

2.5. Phytoplankton biomass, size-composition and chl *a*

Phytoplankton standing stocks were assessed using chl *a* concentrations in the euphotic zone, and further

investigated using microscopy-based estimates of cell biomass classified into 4 size groupings: <2, 2–10, 10–20 and >20 µm cells. NPSG data were downloaded from https://hahana.soest.hawaii.edu/hot/hot_jgofs.html and only data from cruises conducted in June–September from the years 2004, 2008, 2009 and 2010 were used due to availability and data reliability, and to match summer zooplankton data, since isotope data was also from summer cruises. CRD data are from https://www.bco-dmo.org/ and previously published (Taylor et al. 2016), and CCE data from http://cce.lternet.edu/data/cruises. Data for EqP has been previously published (Taylor et al. 2011, Taylor & Landry 2018). All studies followed similar methodology. Briefly, water for pigment assessment was collected using a Niskin-CTD Rosette from 6–8 depths spanning the euphotic zone, filtered onto 25 mm Whatman GF/F filters, and frozen at −20°C, allowing pigments to be extracted in acetone over 24 h at −20°C. Chlorophyll measurements were conducted using a Turner fluorometer following established protocols (Lorenzen 1967). Samples for microscopy were collected from the same depths, and methods are explained in detail in Taylor & Landry (2018). Typically, 500 ml of sample were collected from the CTD and preserved with Lugol's (260 µl), formalin (10 ml) and sodium thiosulfate (500 µl). Samples were stained using proflavine (1 ml 0.33% w/v) and 4′,6-diamidino-2-phenylindole (DAPI, 1 ml of 0.01 mg ml^{-1}), and subsequently filtered onto 25 mm black polycarbonate filters with 0.8 µm (50 ml) and 8 µm (450 ml) pores. Each filter was then mounted onto a glass slide, covered with immersion oil, and imaged under epi-fluorescence using a Zeiss Axiovert 200 M inverted compound microscope equipped with epi-fluorescence microscopy. Images were processed and analyzed using ImagePro software. Cell biovolumes were calculated using the formula for a prolate sphere. Biomass was calculated using conversion equations from Menden-Deuer & Lessard (2000).

3. RESULTS

3.1. Environmental conditions

Temperature and salinity were very different among these regions. The CRD had the warmest surface ocean conditions (28°C) and was the most strongly stratified, with an MLD of 20–30 m. The CCE, a temperate coastal environment, was characterized by cooler temperatures (13°C at the surface) and weaker stratification with a mixed layer in the upper 50 m. The EqP and NPSG locations were also characterized by higher temperatures (25, 24.5°C), deeper MLDs of ~70 and 100 m, respectively, and higher surface salinities (Fig. 3).

Differences in productivity were evident in both maximum chl *a* concentrations and the size composition of phytoplankton. CRD had maximum chl *a* values of ~0.5 µg l^{-1}, with <2 µm contributing about half of the total phytoplankton biomass, followed by 2–10 µm cells (Fig. 4a). In the CCE, minimum chl *a* was an order of magnitude higher than the other 3 regions, and >20 µm cells predominated especially when chl *a* was high (Fig. 4b). EqP had similar maximum chl *a* to CRD despite slightly higher average biomass concentrations, and the 2–10 and 10–20 µm cells dominated the community (Fig. 4c). NPSG had the lowest phytoplankton standing stock (maximum chl *a* = 0.32 µg l^{-1}), with 2–10 µm cells exceeding the biomass contribution of larger cells (10–20 and >20 µm) by at least 1 order of magnitude (Fig. 4d).

3.2. Zooplankton biomass and isotopic baseline variability

Zooplankton standing stocks and $\delta^{15}N$ isotopic values were different among the central ocean areas, NPSG and EqP, and those along the eastern Pacific margin, CCE and CRD. Zooplankton biomass was lowest in the NPSG, EqP had somewhat higher estimates, and CRD and CCE had the highest stocks. Following these patterns in biomass, $\delta^{15}N$ values were lowest (most depleted) in the NPSG (2–5‰), CRD and CCE locations had the highest and most variable $\delta^{15}N$ values (8–13‰), and EqP had intermediate values (5–8‰) (Fig. 5a). Carbon isotope values were largely similar among locations, with the largest variability in $\delta^{13}C$ in the CCE during P1106 (Fig. 5b).

CSIA-AA measurements were limited to 2 tows per location. The source AA index allowed the investigation of the dependence of consumer $\delta^{15}N$ on baseline values. Bulk $\delta^{15}N$ values among the different ecosystems were reasonably correlated with the source AAs (Fig. 6a). A clear separation was observed between NPSG and EqP in their source AAs. Overlap in the bulk values were observed between the 2 mm NPSG zooplankton and the EqP zooplankton — an example of how CSIA-AA can help disentangle discrepancies between baseline variability and trophic enrichment, particularly when this variability is small. Consistent with the patterns observed for the bulk ^{15}N, the source AAs also showed some overlap

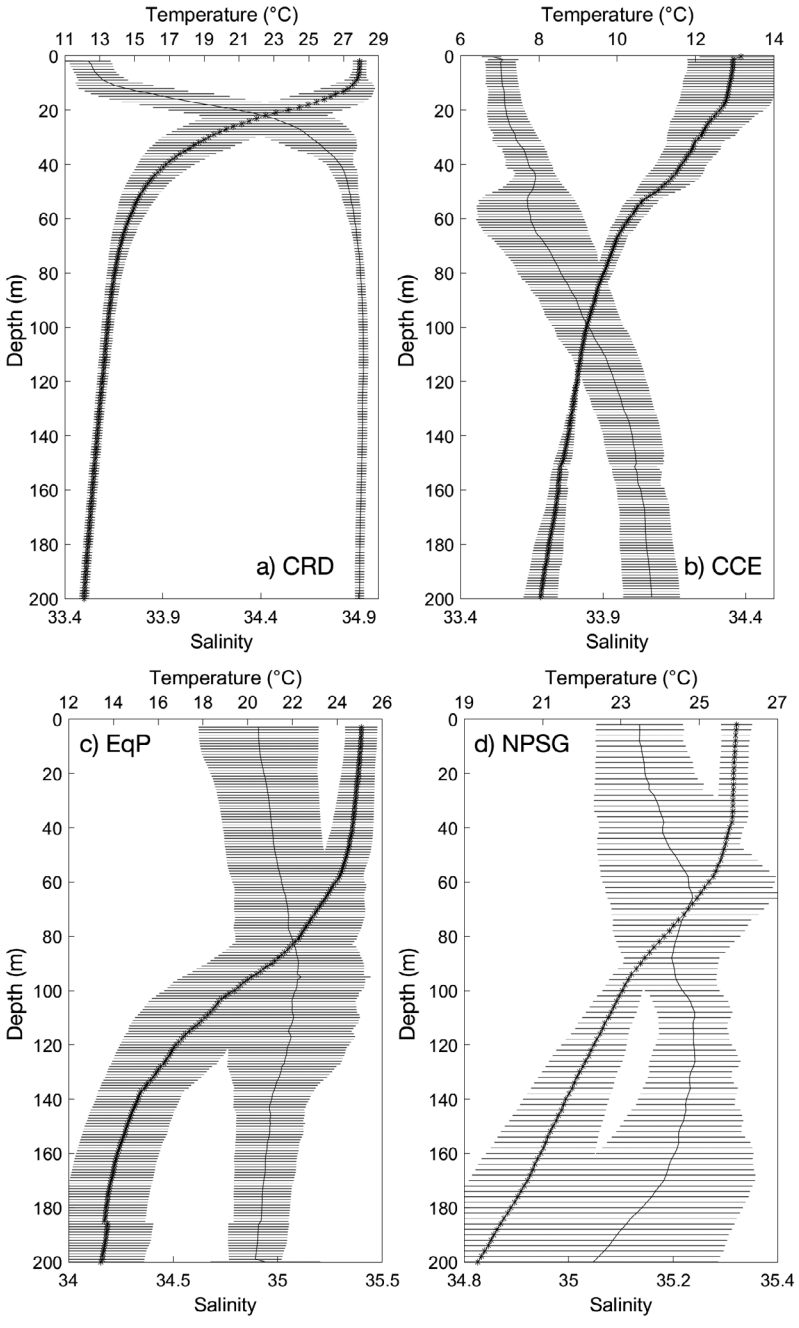

Fig. 3. Temperature (•) and salinity (—) (mean ± SD) for the upper (200 m) ocean in the study regions (a) CRD, (b) CCE, (c) EqP and (d) NPSG. Note different salinity and temperature scales among the 4 graphs

between CRD and CCE, although interestingly, the CCE source AAs had higher $\delta^{15}N$ than CRD (Fig. 6a).

A ~2‰ range in source values was typically observed among samples from each system, although CCE had the largest range of 4‰, suggesting some differences in the baseline of different size classes (Fig. 6a). Investigation of small changes in both metazoan and protistan pathways (McClelland & Montoya 2002, Décima et al. 2017, Landry & Décima 2017) was not possible because of the lack of Phe, yet by using average trophic AA and source AA $\delta^{15}N$ and a traditional TEF of 7‰, it was possible to estimate the TP of the different zooplankton size classes, which ranged rather narrowly between 2 and 3, and was at most 0.9 TP (less than 1 full level) between the smallest and largest size classes (Fig. 6b).

3.3. Zooplankton size and trophic structure

Patterns and absolute values of $\delta^{15}N$ were distinctly different among zooplankton size classes in the systems investigated. The CRD was unique in having an offset in daytime and nighttime isotopic values, with the latter enriched, on average, by 0.5 to 2‰ (Fig. 7a). The smallest and largest size classes during C4 were the only exceptions to this general pattern. Discerning diel patterns within CCE were less straightforward because sampling was not evenly distributed between day and night among the different cruises. The 3 nighttime samples from P0704 had similar patterns, with monotonically increasing $\delta^{15}N$ values from the 0.2–0.5 to 1–2 mm fractions, and the largest size class (2–5 mm) having $\delta^{15}N$ similar to the 0.2–0.5 mm size, suggesting herbivory for these larger animals (Fig. 7b). The daytime P0704 tow was distinctly different, with the 2–5 mm size class having the highest $\delta^{15}N$ values, suggesting a TL increase. The other 2 cruises, P0605 and P1106, had $\delta^{15}N$ values that were higher overall by 1–3‰, further showing how much the baseline (phytoplankton and/or nitrogen source) can vary with different seasons or years in the same region. P0605 isotope patterns generally followed a monotonic increase with size (except for 1 tow; Fig. 7b). Finally, P1106 had intermediate $\delta^{15}N$ values, with each tow showing different patterns with size.

Equatorial zooplankton $\delta^{15}N$ patterns differed between years (cruises). During EB04 (December 2004), zooplankton nitrogen isotope values were

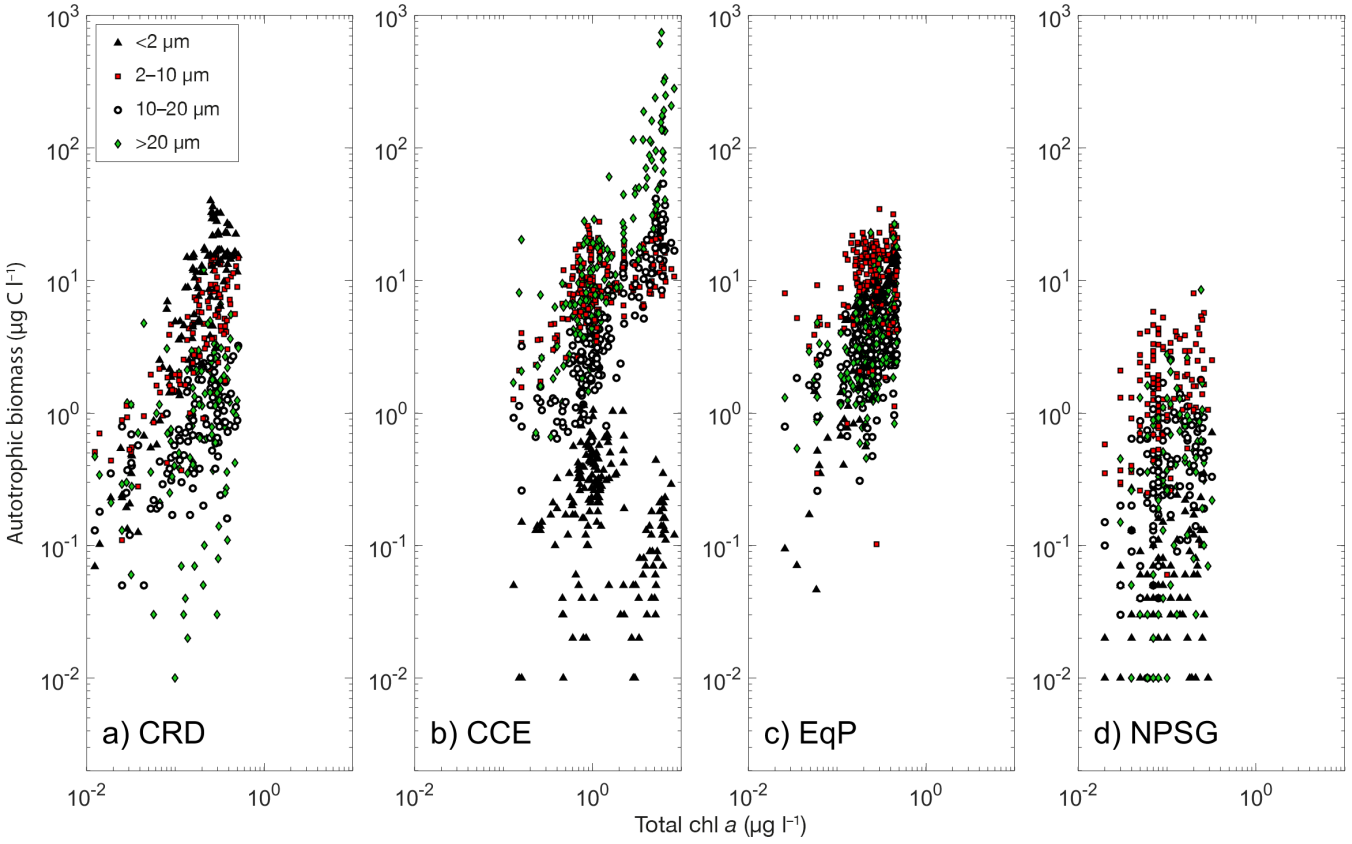

Fig. 4. Phytoplankton community biomass and water column chl *a* throughout the euphotic zone, for (a) CRD, (b) CCE, (c) EqP and (d) NPSG. Phytoplankton biomass was estimated using microscopy and cells were binned into 4 size classes

enriched compared to EB05 by 1–2‰. Communities during the day and nighttime looked generally similar, but during EB04, the largest size (2–5 mm) had higher nighttime nitrogen isotope values at 2 of the 3 stations (Fig. 7c), with the third station showing slightly higher daytime values across all sizes. The community showed a general increasing trend with size — increasing between 1.5 and 2‰ across the 4 size classes — although the largest size class sometimes showed a plateau or even decrease in values during the daytime. Values during EB05 were lower in absolute terms, with the smallest zooplankton at 4–5‰ compared to 5.5–6.5‰ during EB04. The range covered by the different sizes was also depressed, increasing 1‰ from 0.2 to 1 mm, with the largest size class (2–5 mm) typically the same or depleted in ^{15}N compared to 1–2 mm zooplankton.

Zooplankton from NPSG had patterns that were largely consistent between day:night pairs as well as across cruises. The largest zooplankton in this oligotrophic ecosystem consistently had the highest δ^{15}N values of the community, with no distinct differences in this pattern between day and night communities. While nitrogen got progressively enriched in ^{15}N with

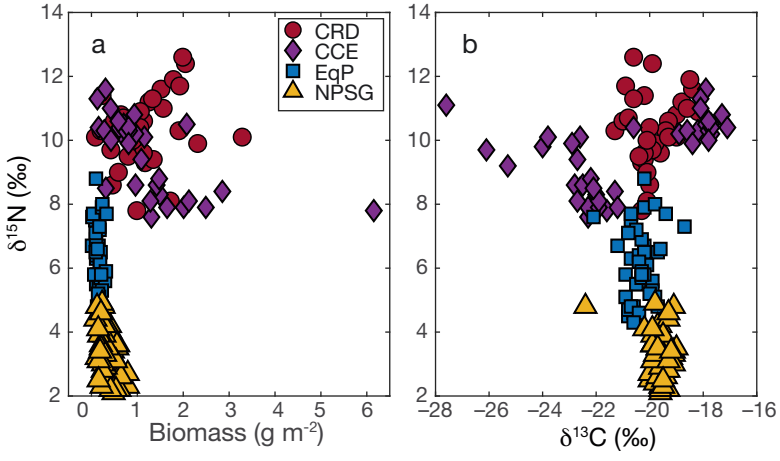

Fig. 5. δ^{15}N values of size-fractionated (each point corresponds to 1 size fraction from 1 tow) zooplankton in the CRD, CCE, EqP and NPSG, plotted vs. (a) biomass of each size class, and (b) δ^{13}C. Note that the abnormally low CCE δ^{13}C values, <–24‰, were from the summer

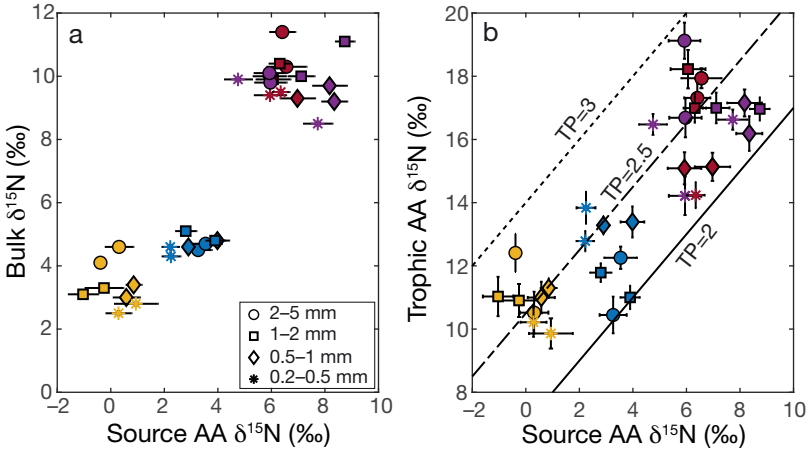

Fig. 6. Compound-specific isotope analysis of amino acids (AAs) and bulk $\delta^{15}N$. (a) Source AAs plotted vs. bulk values, and (b) source AAs vs. trophic AAs (error bars: SD of 3 injections for AA $\delta^{15}N$ measurements). Lines indicate trophic position (TP) = 2, 2.5 or 3. Colors correspond to ecosystems as in Fig. 5. Lowest source values correspond to NPSG, followed by EqP, and CCE/CRD have the highest and overlapping $\delta^{15}N$

increasing size, there was often also a large increase between the 0.2–0.5 and 0.5–1 mm size class (Fig. 7d). The 3 NPSG cruises varied about 0.5‰ at the base (smallest zooplankton size) across the 3 cruises, despite being conducted in different years (all in late summer).

3.4. Isotopic enrichment and trophic difference among zooplankton size classes

The 4 systems showed distinct differences in how the $\delta^{15}N$ values changed among zooplankton size classes. $\Delta^{15}N$ differences between the smallest zooplankton and different size classes ranged from –1 to 3.5‰, considering all ecosystems, although average values ranged between 0.5 and 1.5‰ (Fig. 8a). I first tested if the $\Delta^{15}N$ of each size step was significantly different from zero, which would indicate a difference between the smallest (0.2–0.5 mm) and the >0.5 mm zooplankton assemblage. In the EqP and NPSG, there was a $\Delta^{15}N$ difference between the smallest zooplankton and the 3 larger size classes (Fig. 8, Sign test, $p < 0.05$). For the eastern Pacific locations, the CCE showed no difference between the smallest zooplankton and the larger sizes, and the CRD showed a statistical increase in $\Delta^{15}N$ for the 1–2 mm size class. Interestingly, the $\Delta^{15}N$ of the 2–5 mm CRD zooplankton was not significantly different from zero, suggesting a group of large herbivorous zooplankton was at least contributing to this size class. Evaluating the difference among size steps, a Kruskal-Wallis analysis indicated that differences among the organisms larger than 0.5 mm were significant only for NPSG and EqP. EqP showed a trophic increase between 0.5–1 and 1–2 mm zooplankton, and the NPSG showed a $\Delta^{15}N$ difference between 1–2 and 2–5 mm organisms. Thus, zooplankton in the EqP and NPSG showed 2 statistically significant $\Delta^{15}N$ increases within the assemblage, CRD had 1, and zooplankton in the CCE were all at the same TL on average. Interestingly, the NPSG was the only system where the largest zooplankton had significantly higher $\Delta^{15}N$ (Fig. 8a).

Patterns in $\Delta^{13}C$ with size were consistent with a lack of trophic enrichment (Fig. 8b). The only significant differences that were observed occurred in EB zooplankton, with lower $\Delta^{13}C$ associated with the largest zooplankton, potentially suggesting differences in the source (phytoplankton groups). In the other 3 systems, $\Delta^{13}C$ values were consistent across sizes and not significantly different from the 0.2–0.5 mm zooplankton, suggesting relatively similar baselines for the whole community.

TPs calculated using CSIA-AA were higher than those calculated using bulk data (Fig. 9a), and the range for all TP_{AA} estimates was larger (0.9) compared to TP_{bulk} (0.6). While this study assumes a $TP_{bulk} = 2$ for the 0.2–0.5 mm size class, TP_{AA} for these small organisms ranged from 2.1 to 2.7, with a mean of 2.4 across all 4 ecosystems (Fig. 6b, Tables S5 & S6). However, high variability and low sample size (2 per ecosystem) prevented the use of TP_{AA} for investigating patterns in trophic structure with size. TP_{bulk} values averaged for each ecosystem and size class indicated a range of 0.5 TP for the entire zooplankton assemblage (Fig. 9b).

3.5. Zooplankton biomass

Among the ecosystems sampled, CCE and NPSG are end members in productivity regimes, supporting the highest (CCE) and lowest (NPSG) phytoplankton biomass (Fig. 3) and PP (Table 1), as well as the steepest (CCE) and flattest (NPSG) slopes of the NBSS (Figs. 10 & 11). CRD and EqP are intermediate, with intermediate NBSS slopes. CCE had the largest variability among sampling times and locations, followed by EqP. CRD and NPSG displayed the least

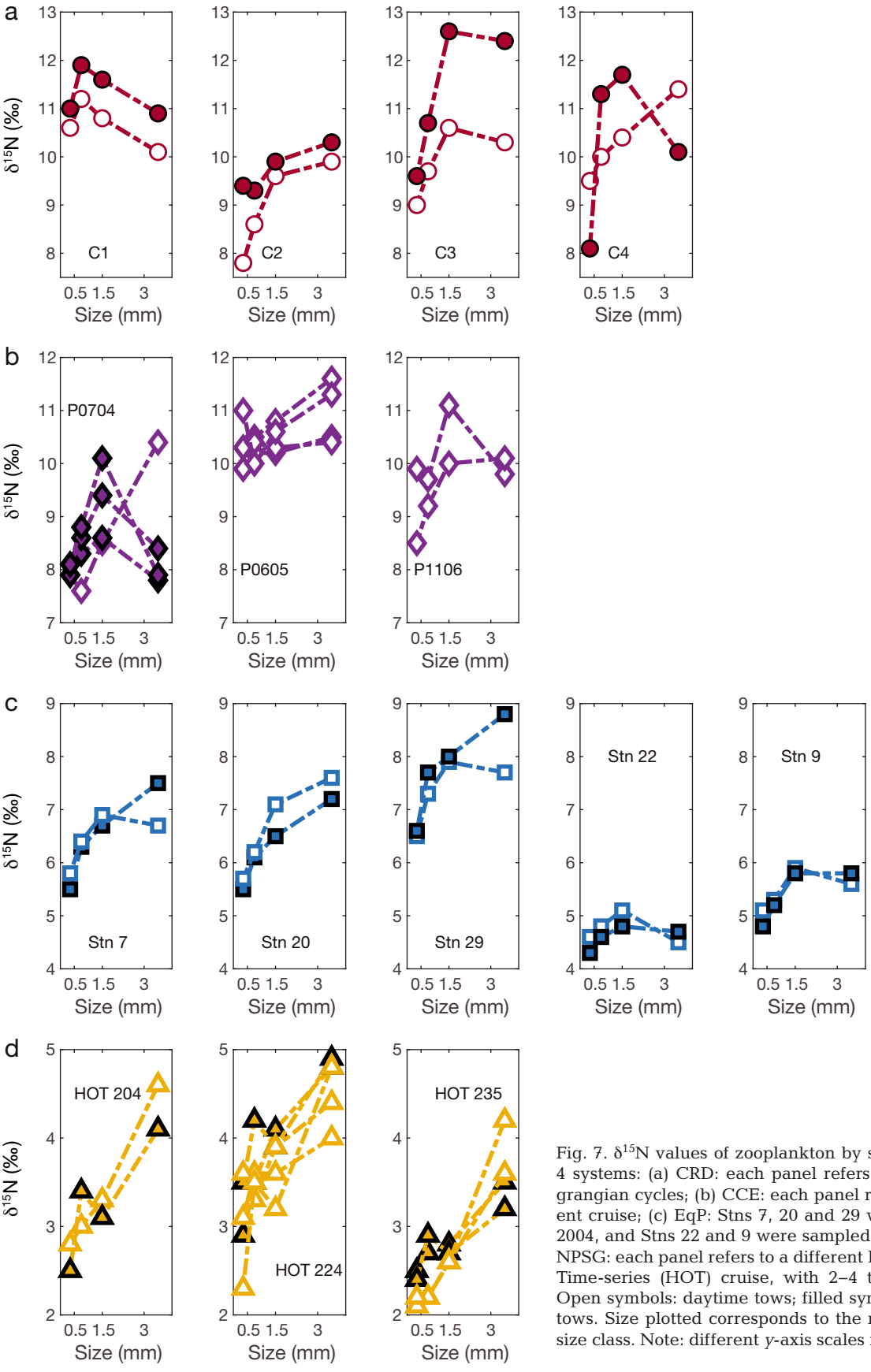

Fig. 7. $\delta^{15}N$ values of zooplankton by size class for the 4 systems: (a) CRD: each panel refers to different Lagrangian cycles; (b) CCE: each panel refers to a different cruise; (c) EqP: Stns 7, 20 and 29 were sampled in 2004, and Stns 22 and 9 were sampled in 2005; and (d) NPSG: each panel refers to a different Hawaiian Ocean Time-series (HOT) cruise, with 2–4 tows per cruise. Open symbols: daytime tows; filled symbols: nighttime tows. Size plotted corresponds to the mid-size of each size class. Note: different *y*-axis scales for each location

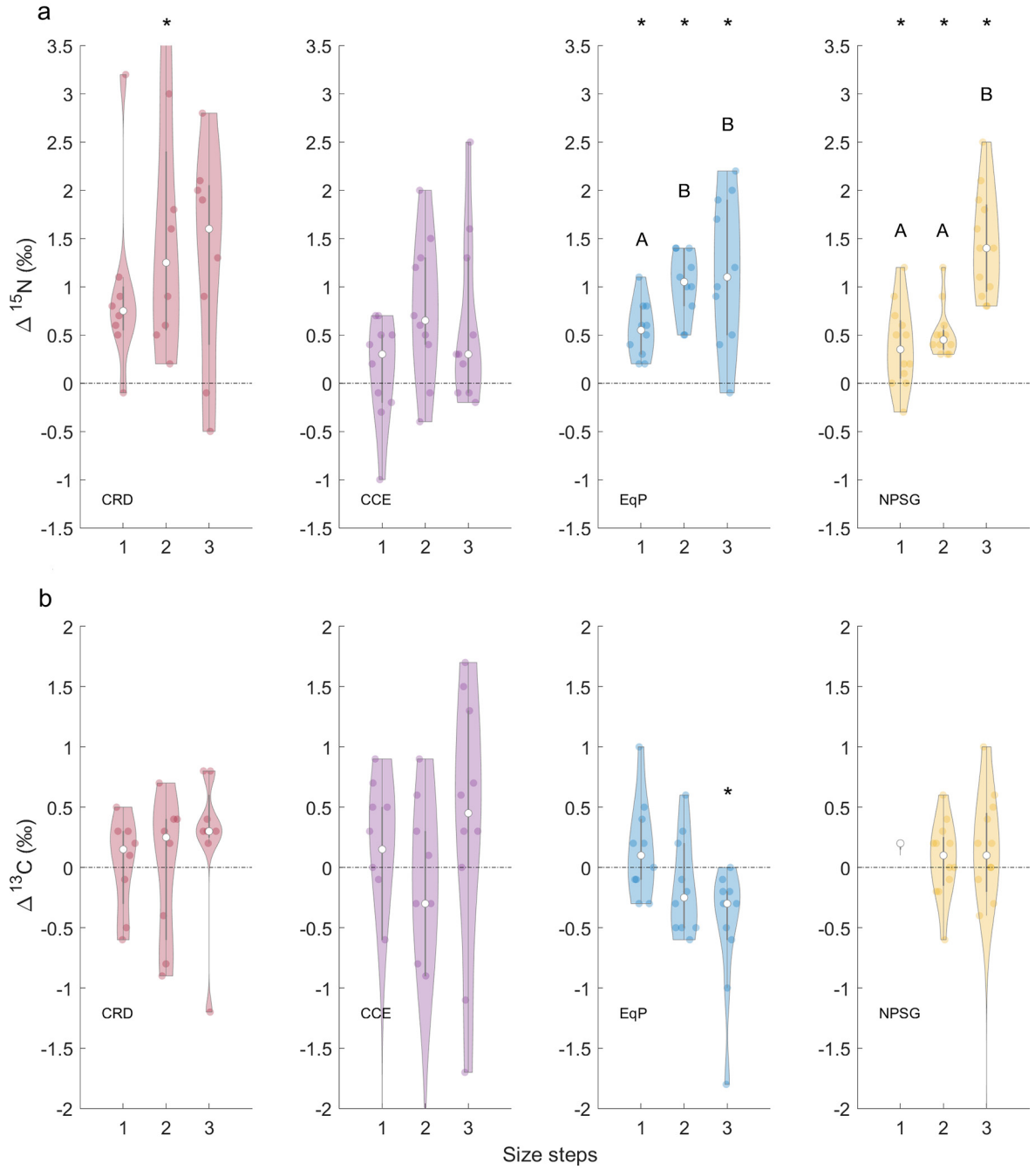

Fig. 8. Violin plots of isotopic differences among size classes for CRD, CCE, EqP and NPSG. (a) $\Delta^{15}N$ reflects difference between $\delta^{15}N$ of the smallest zooplankton size (0.2–0.5 mm) with each of the larger size classes: 0.5–1 mm (step 1), 1–2 mm (step 2) and 2–5 mm (step 3). (b) $\Delta^{13}C$ is the same calculation, but based on $\delta^{13}C$. *Significantly different from zero vs. the 0.2–0.5 mm size class. Different letters (A, B) indicate significant differences in $\Delta^{15}N$ among size steps

variability in biomass distribution with sizes. Three of the 4 systems (EqP being the exception) had statistically significant different slopes and intercepts for day and night communities (ANCOVA, $p < 0.05$), with nighttime slopes shallower (greater contribution of larger organisms) than daytime (Fig. 10). CRD and CCE were characterized by an overall monotonic decrease in normalized biomass with size, while EqP and NPSG often had similar values for the 2 smallest sizes. The slopes of the NBSS for the day/night averaged biomass varied different among systems. CCE had the steepest slope and was significantly different

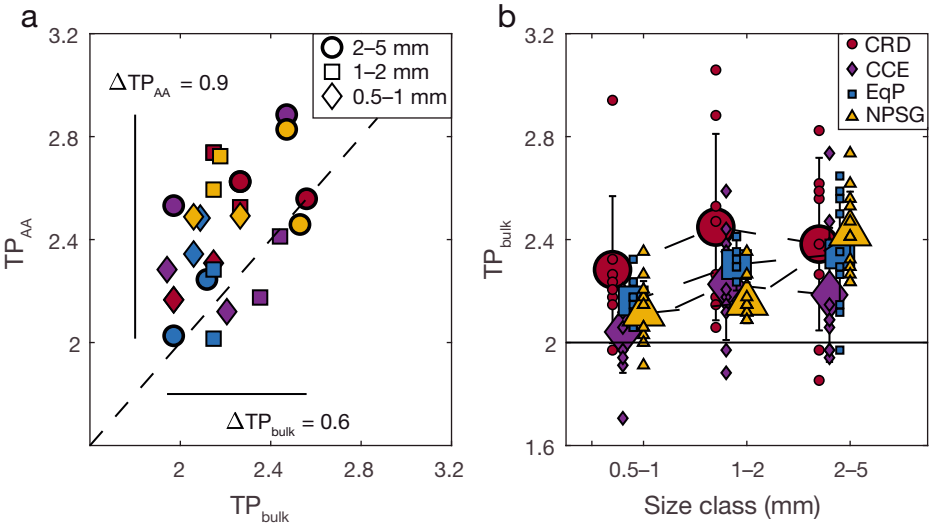

Fig. 9. (a) Trophic positions (TPs) based on compound-specific isotope analysis of amino acids (AAs) (TP_{AA}) vs. TPs based on bulk values (TP_{bulk}); symbols: size classes; colors: ecosystems as in panel b. (b) TP_{bulk} for each size step; symbols and colors indicate ecosystems (mean ± SD of all samples)

from CRD and NPSG. The oligotrophic NPSG had the flattest slopes, significantly different from EqP and CCE (ANCOVA, $p < 0.05$).

Zooplankton total biomass was highest in the CRD and CCE, followed by EqP, and NPSG (Fig. 12a). However, variability in the CCE was such that 1 cruise (P0704) had the highest biomass of all cruises/locations sampled, but the second spring cruise (P0605) had about half the average zooplankton biomass. The $\log_{10}$(zoo:phyto) was highest for CRD, and interestingly, similar for CCE and NPSG, with EqP displaying the lowest ratio (Fig. 12b). Zooplankton biomass was generally inversely correlated with phytoplankton biomass for the 3 upwelling (advective) systems — CRD, CCE and EqP (Fig. 12).

4. DISCUSSION

4.1. Baseline variability

The main driver in zooplankton $\delta^{15}N$ variability was due to baseline conditions (Figs. 5a & 6a), which was unique to 3 of the 4 marine ecosystems evaluated in this study (Kruskal-Wallis, $p << 0.05$); CCE and CRD had high and overlapping $\delta^{15}N$ that were indistinguishable from each other. These substantial differences in baseline values are related to the sources of bioavailable nitrogen to the biological community. Variability in the spatial and temporal dynamics that regulate nitrogen uptake can additionally lead to ~2‰ changes in baseline $\delta^{15}N$ within each large ecosystem. This can be observed in the spatial differences within CRD (Fig. 7a) and temporal differences associated with sampling in different years in CCE and EqP (Fig. 7b,c). Shifts of ~2‰ have been previously documented in studies investigating the effects of El Niño on the California Current (Rau et al. 2003, Ohman et al. 2012, Décima et al. 2013). The very large range in baseline $\delta^{15}N$ values confirms that it is essential to normalize by these before it is possible to investigate the much smaller differences that arise through trophic enrichment or local perturbations to the ecosystem.

The limited day/night differences in isotopes is surprising given the expectation that vertical migrants consist of largely predatory taxa. These results suggest that the migrating communities comprise a similar combination of herbivores/omnivores/carnivores as the resident communities, thus not significantly altering isotopic values despite significant migrant biomass (e.g. Décima et al. 2011, 2016, Valencia et al. 2018). The main exception to this pattern seems to be within CRD, where nighttime values are typically enhanced but patterns largely mirror those of the day-

Table 1. Summary of primary production (PP, mean ± SD) for each region, averaged from the studies presented here. CCE: California Current Ecosystem; CRD: Costa Rica Dome; EqP: Equatorial Pacific; NPSG: North Pacific Subtropical Gyre; n: number of zooplankton tows analyzed for biomass; NA: not applicable

Region	Integrated PP (mg C m^{-2} d^{-1})	No. of cruises	No. of cycles	No. of stations	Years	n
CCE	2677 ± 1502	2	3, 2	NA	2006, 2007	20
CRD	1029 ± 157	1	4	NA	2010	16
EqP	867 ± 96	2	NA	16, 14	2004, 2005	30
NPSG	569 ± 119	10	NA	1	2004–2014	31

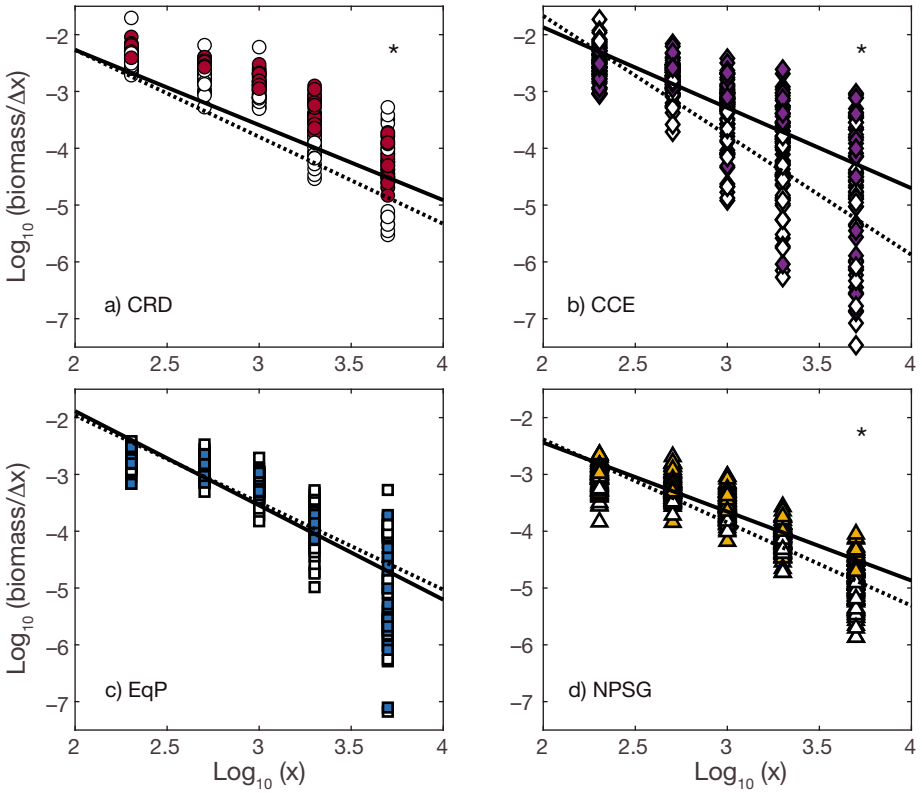

Fig. 10. Biomass (log-transformed and normalized by size bin) plotted against zooplankton size classes (log-transformed; 'x': size classes 0.2, 0.5, 1, 2 and 5 mm) for (a) CRD, (b) CCE, (c) EqP and (d) NPSG. Open symbols: daytime tows; filled symbols: nighttime tows. Note these estimates were done including the additional >5 mm size class. Lines correspond to spectral slope fit for night (solid), day (dotted). *Systems where differences between day and night were significant

time. While this could be due to migrating euphausiids (Décima et al. 2019), patterns from C and N isotopes suggested that most of the crustacean-dominated community was sourcing their carbon from the surface, while nitrogen could be supplied by particles from the surface layer or below the thermocline (Décima et al. 2019). It is difficult to explain the enhanced nighttime $\delta^{15}N$ values without depleted $\delta^{13}C$ values from feeding at depth. Enhanced TLs for migrating zooplankton can be postulated, although the near-mirroring in patterns would require very similar relative contributions of migrants to each size class, or a compensatory effect between TP increase and relative biomass contribution, which is unlikely. Other possible causes could be selective feeding on different (higher $\delta^{15}N$) phytoplankton by nighttime grazers (grazing was higher at night; Décima et al. 2016), or assimilation of heavier nitrogen coming from deeper hypoxic/anoxic waters decoupled from carbon assimilation (Williams et al. 2014, Décima et al. 2019).

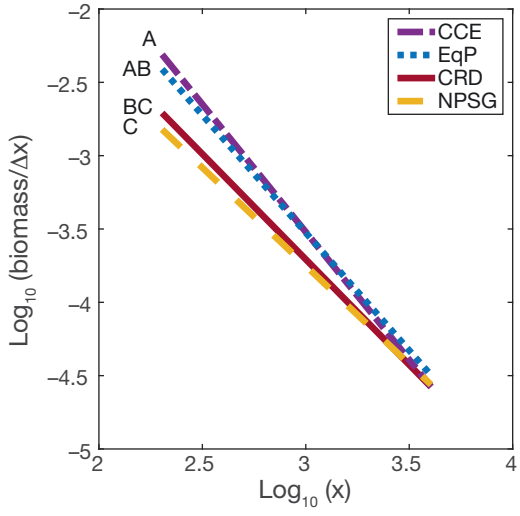

Fig. 11. Slopes of normalized biomass size spectra for each system. Letters (A–C) denote slopes significantly different from each other (ANCOVA, $p < 0.05$)

Source values from AAs confirmed that variation of the baseline drove the large differences in bulk $\delta^{15}N$ values (Fig. 6), in line with previous observations (Décima et al. 2013, Hetherington et al. 2017). The elevated values observed in the CRD and CCE are set by the high $\delta^{15}N$ in the source nitrate (5–15‰) due to denitrification (Sigman et al. 2009, Buchwald et al.

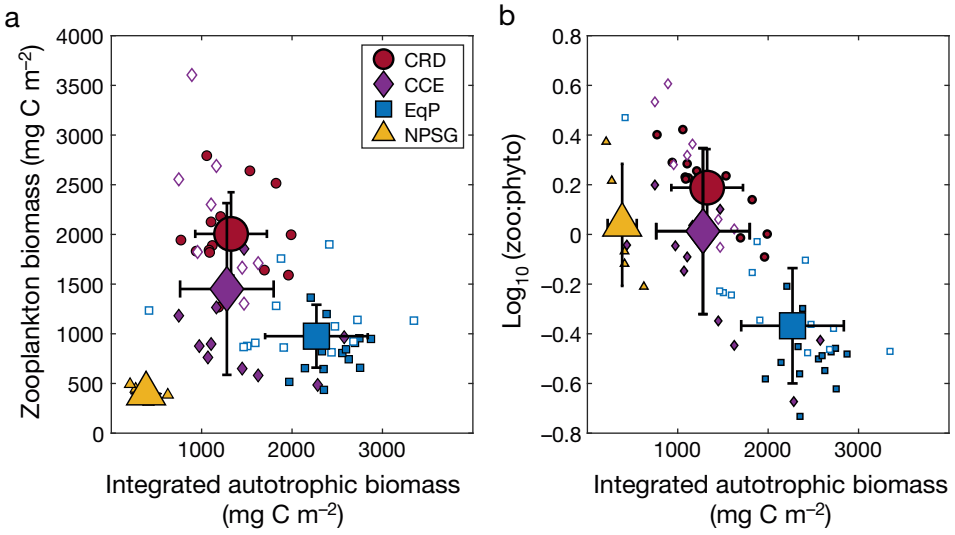

Fig. 12. (a) Upper ocean zooplankton biomass and (b) ratio of zooplankton:phytoplankton biomass ($\log_{10}$(zoo:phyto)) as a function of (euphotic zone) integrated autotrophic biomass. Small symbols: individual measurements; large symbols: means (±SD)

2015) that occurs in deeper waters where conditions can be hypoxic (CCE) or virtually anoxic (CRD). These 2 systems are also are linked in their source waters (Liu & Kaplan 1989). Upwelled nitrate also fuels production in EqP, yet the lower absolute values suggest lighter nitrate (~6‰) and the lack of significant denitrification. In contrast, the low $\delta^{15}N$ values in the subtropical North Pacific are likely a consequence of N_2 fixation, which can fuel up to half the PP during the summer in the oligotrophic gyres (Karl et al. 1997, Wang et al. 2019). NPSG zooplankton baseline (0.2–0.5 mm size) values were intermediate (2–3.5‰) between the N_2 fixation isotopic value (~0‰) and upwelled nitrate (~6‰), consistent with the importance of both sources to biological production (Dore et al. 2002), particularly in the summer when nitrogen fixation results in a phytoplankton bloom (Church et al. 2009). These depleted isotopic values have also been observed in plankton in the North Atlantic Sargasso Sea, where N fixation is an important process in providing biologically available N (McMahon et al. 2013).

4.2. Trophic structure and phytoplankton size composition

Investigating trophic steps by using statistically significant differences in $\Delta^{15}N$ was done because of the high variability in isotope data (Fig. 8). It should be noted that this high variability is not uncommon (Mompean et al. 2013, Williams et al. 2014, Hunt et al. 2015), and is likely due to both changes in diets of component zooplankton, as well as changes in the composition of animals contributing to each size classes on these spatial and temporal scales. While I have not seen this approach taken before, it provides an objective approach to answer interregional differences in trophic structure in the zooplankton community. Based on these differences, predictions of shorter/longer food chains related to productive/oligotrophic environments, respectively, held when considering the most (CCE) and least (NPSG) productive systems (Table 1). That the CCE environment, with order-of-magnitude higher chl *a* concentrations and dominance of >20 µm cells, showed no significant trophic steps within the zooplankton community, suggests that carnivory, on average, was not a substantial trophic pathway (Fig. 8a) during this sampling time. Zooplankton spanning 1 order of magnitude in size were primarily grazing on phytoplankton and/or microzooplankton. This underscores that these highly productive areas of the CCE, with high biomass of large phytoplankton, are largely dominated by herbivorous–omnivorous pathways, at least in the spring (Legendre & Rassoulzadegan 1995, Landry et al. 2009). The NPSG, on the low end of the productivity spectrum, had 3 significant steps within the community, and was the only system where large (2–5 mm) zooplankton fed at a significantly higher TL, supporting a longer food web within metazoan plankton in the oligotrophic environment.

While CRD and EqP had intermediate values of PP, EqP did have substantially higher integrated standing stocks of phytoplankton (Fig. 12) because the euphotic zone was so much deeper (Taylor et al. 2011), and production in the CRD had high contributions of picophytoplankton which are not as directly available to zooplankton. However, the number of trophic differences within the EqP zooplankton was comparable to the NPSG, not CRD. These 2 systems (EqP and CRD) provide interesting conditions to fur-

ther explore the drivers of zooplankton trophic structure. Both systems had similar PP values (Table 1) during these studies (Landry et al. 2011, 2016). However, CRD did have slightly higher PP, but was characterized by a phytoplankton size composition dominated by smaller cells (Fig. 4a) and lower integrated phytoplankton biomass (Fig. 12), and conversely higher zooplankton standing stocks (Figs. 5a & 12a) and fewer trophic steps (Fig. 8a). Previous investigations have shown higher grazing in the CRD based on gut pigment data (Décima et al. 2011, 2016), and the $\log_{10}$(zoo:phyto) confirmed high TE between zooplankton and phytoplankton, which is in line with results from mass-balance (Landry et al. 2016) and linear inverse models (Stukel et al. 2018). A unique and fundamental characteristic of the CRD is a very shallow MLD (Fig. 2) which effectively concentrates PP into a compressed vertical habitat, and previous studies showed that CRD epipelagic zooplankton were indeed sourcing their food from the upper 30 m (Décima et al. 2019). A compressed vertical habitat can lead to enhanced zooplankton encounter rates with prey particles, and among particles, increasing aggregate formation and average particle size, ultimately enhancing TE. This equates to an increase in productive space (total ecosystem productivity adjusted for ecosystem size) in the vertical dimension, which has also been proposed as an important factor driving food-chain length (Schoener 1989).

Interpreting $\Delta^{15}N$ in EqP suggests that despite the system being fueled by upwelled nitrate, and having high standing stocks of phytoplankton and higher levels of herbivory in 2004/2005 (Décima et al. 2011) compared to 1992 (Dam et al. 1995), the zooplankton community is still characterized by high levels of carnivory, which is consistent with conclusions based on metabolic calculations and inverse modeling (Dam et al. 1995, Roman et al. 1995, 2002, Landry et al. 2020). In addition, similarities between the $\Delta^{15}N$ for EqP and NPSG could be due to taxonomic composition. While the species compositions were not available for all the studies presented here, and can thus only be briefly discussed in light of past studies, both EqP and the NPSG have generally similar compositions, with a zooplankton community dominated by copepods, and lacking large suspension-feeding zooplankton such as euphausiids and thaliaceans (Hayward 1980, Roman et al. 1995, Landry et al. 2001), which are present in the CCE and CRD (Fernandez-Alamo & Farber-Lorda 2006, Lavaniegos & Ohman 2007, Décima et al. 2016, 2019). It should be noted that the present study focuses on the non-thaliacean zooplankton community, as animals >5 mm were not included in the analysis, although in general they were also not sampled in high abundances during these specific oceanographic voyages. Pyrosomes are important ecologically in the CRD, but only comprised 3% of the zooplankton community biomass (e.g. Decima et al. 2019).

While the hypothesis that a shallow MLD contributes to the higher trophic transfer in CRD vs. EqP (despite similar productivity and smaller phytoplankton) remains untested, this mechanism is particularly relevant in light of documented long-term changes accompanied by secular warming due to climate change. Long-term increases in zooplankton biomass have been reported for NPSG (Sheridan & Landry 2004, Valencia et al. 2016), EqP (Décima et al. 2011) and the CCE (Lavaniegos & Ohman 2003, Ohman et al. 2009). Additionally, a similar long-term increase in zooplankton standing stocks has been reported in the Bermuda Atlantic Time-Series site in the oligotrophic Sargasso Sea (Steinberg et al. 2012). While a single explanation for increasing zooplankton standing stocks in these disparate regions (characterized by different nutrient limitations) is unlikely, it is noteworthy that one driver of enhanced TE is the size of the vertical habitat, which can become compressed with enhanced stratification in warming waters (Li et al. 2020). Understanding and predicting future changes due to increasing global temperatures will require careful consideration of the multiple, contrasting drivers including changes in physical forcing, phytoplankton size and community composition, habitat characteristics, and the composition of the zooplankton assemblage.

4.3. Zooplankton biomass, NBSS and TE

Calculation of NBSS from only 5 size points (Figs. 11 & 12) can be reasonably questioned, since more robust estimations can be drawn from a greater number of size categories. However, in a study in the CCE region, Rykaczewski & Checkley (2008) used the same 5-point approach to investigate patterns in NBSS across varying conditions of upwelling and system productivity, and subsequently arrived at the same conclusion by using high size-resolution Zooscan data that provided a greater number of size bins for slope calculations (Rykaczewski 2019). Regardless of the number of bins, although particularly when there are few, results must be interpreted with caution because a variety of ecosystem factors, in addition to PP, can affect the size distribution of the zooplankton assemblage.

NBSS differences among systems was consistent with isotope results, identifying CCE and NPSG as the 2 extremes within this interregional comparison. However, NBSS highlighted similarities between CCE–EqP, and CRD–NPSG, in contrast to system similarities observed for $\Delta^{15}N$, which grouped similar areas as EqP–NPSG and CCE–CRD. Estimates of TE using $\log_{10}$(zoo:phyto) also ranked CRD and CCE at the top, although NPSG (despite low zooplankton biomass) was just as efficient, and the only system with significantly lower TE was EqP.

Similarities between CCE and EqP (Fig. 11) can be interpreted considering Ekman-driven upwelling results in important diatom production in both systems (Brzezinski et al. 2008, Venrick 2012) as well as temporal and spatial variability in the compositional and size balance of zooplankton (Vinogradov & Shushkina 1978). While typical interpretations of NBSS slopes suggest shallower slopes for more productive areas (Zhou 2006, Rykaczewski & Checkley 2008), our observations are opposite to this expectation (Fig. 11). Other studies have also concluded that steeper NBSS slopes do not always indicate reduced trophic TE. Zhou et al. (2009) reported steeper slopes in more productive conditions when zooplankton was dominated by smaller herbivorous taxa, and flatter slopes when the community was dominated by omnivorous-carnivorous taxa. Thus, other factors such as seasonality in growth and non-steady state conditions can substantially affect these metrics and consequent interpretations of the slope (Marcolin et al. 2013). On the opposite end of the spectrum, the ecosystem that exhibits the least pronounced seasonality is the NPSG (Hayward et al. 1983, Landry et al. 2001, Bidigare et al. 2009, Valencia et al. 2016) and the flatter slope can be interpreted as due to higher biomass of large carnivores, consistent with results from the isotope data. Interestingly, this resulted in a TE that was comparable to that estimated for CCE and CRD (Fig. 12b), and is consistent with other studies reporting relatively higher TE in low-biomass and nutrient-poor regions (Bradford-Grieve et al. 2003, San Martin et al. 2006).

Patterns in $\log_{10}$(zoo:phyto) suggests factors in addition to trophic structure and size composition can affect TE. However, the use of $\log_{10}$(zoo:phyto) as a proxy to compare TE (which is strictly defined by production of these 2 groups, not biomass) among ecosystems is less robust if the ecosystems in question have different top-down forcing, or have significant advection that leads to a decoupling of PP and zooplankton biomass. Since zooplankton standing stocks are a result of the starting zooplankton biomass, the rate of increase (production, consequent of TE) and mortality, areas with stronger predation and/or advection will have different loss terms affecting $\log_{10}$(zoo:phyto). To my knowledge, given high consumer biomass in both the CCE and CRD (Ballance et al. 2006, Barlow et al. 2008, Davison et al. 2013), it is unlikely that EqP experiences disproportional top-down forcing compared to the other advective systems. More likely is the consequence of the combination of decreased TE via greater trophic steps within the zooplankton community (Fig. 8a) and the advective nature of the system, as the zooplankton community biomass can almost double between the equator and 5° latitude north or south (White et al. 1995), although this was not detected in this study which only sampled within 4° latitude of the equator (Décima et al. 2011).

4.4. Conclusions

This system comparison supports the general observation that highly productive marine systems with large phytoplankton have higher levels of herbivory, while oligotrophic systems with low PP and small-sized cells have more trophic steps within the zooplankton community. Less (more) negative NBSS slopes corresponded to more (less) trophic steps. Patterns in $\log_{10}$(zoo:phyto) suggest TE is a function of multiple factors, including but not limited to trophic structure and PP, and likely affected by other conditions such as advection. While PP extremes were consistent with the highest/lowest values in $\Delta^{15}N$ and NBSS, it is likely that other factors such as physical processes leading to habitat reduction and advection play important roles in determining food-chain length and TE in marine ecosystems. The general paradigm relating food-chain length to production and phytoplankton size composition, while originally formulated considering the phytoplankton–microzooplankton link (Legendre & Rassoulzadegan 1995), does in fact hold when investigating metazoan carnivorous pathways in marine systems at the productivity extremes, yet the implications for TE are more complex.

Data availability. CSIA-AA and bulk data is included in the supplementary tables. Biomass data has been previously published and/or deposited in the different repositories indicated in Section 2.

Acknowledgements. This work would not have been possible without the hard work of crew and scientists on the CRD cruise (R/V 'Melville'); Equatorial Biocomplexity cruises (R/V 'Roger Revelle'); CCE LTER cruises P0605 (R/V 'Knorr'), P0704 (R/V 'Thompson') and P1106 (R/V 'Melville'); and HOT cruises (R/V 'Kilo Moana'). I gratefully acknowledge the assistance of Lisa Della Ripa, Elizabeth Gier and Brian Popp for help with CSIA-AA analyses. Special thanks to Michael Landry and Jennifer Prairie for helpful comments. The manuscript was also greatly improved by the input of 3 anonymous reviewers. The study was supported by National Science Foundation Grants OCE-1260055, -0322074 (EqP), -0826626 (CRD), -1614359 (CCE-LTER) and -1756517 (NPSG).

LITERATURE CITED

Armengol L, Calbet A, Franchy G, Rodríguez-Santos A, Hernández-León S (2019) Planktonic food web structure and trophic transfer efficiency along a productivity gradient in the tropical and subtropical Atlantic Ocean. Sci Rep 9:2044

Ballance LT, Pitman RL, Fiedler PC (2006) Oceanographic influences on seabirds and cetaceans of the eastern tropical Pacific: a review. Prog Oceanogr 69:360–390

Barlow J, Kahru M, Mitchell BG (2008) Cetacean biomass, prey consumption, and primary production requirements in the California Current ecosystem. Mar Ecol Prog Ser 371:285–295

Bidigare RR, Chai F, Landry MR, Lukas R and others (2009) Subtropical ocean ecosystem structure changes forced by North Pacific climate variations. J Plankton Res 31: 1131–1139

Bradford-Grieve JM, Probert PK, Nodder SD, Thompson D and others (2003) Pilot trophic model for subantarctic water over the Southern Plateau, New Zealand: a low biomass, high transfer efficiency system. J Exp Mar Biol Ecol 289:223–262

Brinton E, Townsend A (2003) Decadal variability in abundances of the dominant euphausiid species in southern sectors of the California Current. Deep Sea Res II 50: 2449–2472

Brzezinski MA, Dumousseaud C, Krause JW, Measures CI, Nelson DM (2008) Iron and silicic acid concentrations together regulate Si uptake in the equatorial Pacific Ocean. Limnol Oceanogr 53:875–889

Buchwald C, Santoro AE, Stanley RHR, Casciotti KL (2015) Nitrogen cycling in the secondary nitrite maximum of the eastern tropical North Pacific off Costa Rica. Glob Biogeochem Cycles 29:2061–2081

Calbet A, Landry MR (1999) Mesozooplankton influences on the microbial food web: direct and indirect trophic interactions in the oligotrophic open ocean. Limnol Oceanogr 44:1370–1380

Chikaraishi Y, Ogawa NO, Kashiyama Y, Takano Y and others (2009) Determination of aquatic food-web structure based on compound-specific nitrogen isotopic composition of amino acids. Limnol Oceanogr Methods 7: 740–750

Church MJ, Mahaffey C, Letelier RM, Lukas R, Zehr JP, Karl DM (2009) Physical forcing of nitrogen fixation and diazotroph community structure in the North Pacific subtropical gyre. Glob Biogeochem Cycles 23:GB2020

Dam HG, Zhang XS, Butler M, Roman MR (1995) Mesozooplankton grazing and metabolism at the equator in the central Pacific: implications for carbon and nitrogen fluxes. Deep Sea Res II 42:735–756

Davison PC, Checkley DM, Koslow JA, Barlow J (2013) Carbon export mediated by mesopelagic fishes in the northeast Pacific Ocean. Prog Oceanogr 116:14–30

Décima M, Landry MR (2020) Resilience of plankton trophic structure to an eddy-stimulated diatom bloom in the North Pacific Subtropical Gyre. Mar Ecol Prog Ser 643: 33–48

Décima M, Landry MR, Rykaczewski RR (2011) Broad scale patterns in mesozooplankton biomass and grazing in the eastern equatorial Pacific. Deep Sea Res II 58:387–399

Décima M, Landry MR, Popp BN (2013) Environmental perturbation effects on baseline $\delta^{15}N$ values and zooplankton trophic flexibility in the southern California Current Ecosystem. Limnol Oceanogr 58:624–634

Décima M, Landry MR, Stukel MR, Lopez-Lopez L, Krause JW (2016) Mesozooplankton biomass and grazing in the Costa Rica Dome: amplifying variability through the plankton food web. J Plankton Res 38:317–330

Décima M, Landry MR, Bradley CJ, Fogel ML (2017) Alanine $\delta^{15}N$ trophic fractionation in heterotrophic protists. Limnol Oceanogr 62:2308–2322

Décima M, Stukel MR, López-López L, Landry MR (2019) The unique ecological role of pyrosomes in the Eastern Tropical Pacific. Limnol Oceanogr 64:728–743

DeNiro MJ, Epstein S (1981) Influence of diet on the distribution of nitrogen isotopes in animals. Geochim Cosmochim Acta 45:341–351

Dore JE, Brum JR, Tupas LM, Karl DM (2002) Seasonal and interannual variability in sources of nitrogen supporting export in the oligotrophic subtropical North Pacific Ocean. Limnol Oceanogr 47:1595–1607

du Pontavice H, Gascuel D, Reygondeau G, Maureaud A, Cheung WWL (2020) Climate change undermines the global functioning of marine food webs. Glob Change Biol 26:1306–1318

Fernandez-Alamo MA, Farber-Lorda J (2006) Zooplankton and the oceanography of the eastern tropical Pacific: a review. Prog Oceanogr 69:318–359

Fry B, Quinones RB (1994) Biomass spectra and stable isotope indicators of trophic level in zooplankton of the northwest Atlantic. Mar Ecol Prog Ser 112:201–204

García-Comas C, Sastri AR, Ye L, Chang CY and others (2016) Prey size diversity hinders biomass trophic transfer and predator size diversity promotes it in planktonic communities. Proc R Soc B 283:20152129

Hannides CCS, Popp BN, Landry MR, Graham BS (2009) Quantification of zooplankton trophic position in the North Pacific Subtropical Gyre using stable nitrogen isotopes. Limnol Oceanogr 54:50–61

Hannides CCS, Popp BN, Choy CA, Drazen JC (2013) Midwater zooplankton and suspended particle dynamics in the North Pacific Subtropical Gyre: a stable isotope perspective. Limnol Oceanogr 58:1931–1946

Hayward TL (1980) Spatial and temporal feeding patterns of copepods from the North Pacific Central Gyre. Mar Biol 58:295–309

Hayward TL, Venrick EL, McGowan JA (1983) Environmental heterogeneity and plankton community structure in the central North Pacific. J Mar Res 41:711–729

Hetherington ED, Olson RJ, Drazen JC, Lennert-Cody CE, Ballance LT, Kaufmann RS, Popp BN (2017) Spatial food-web structure in the eastern tropical Pacific Ocean based

on compound-specific nitrogen isotope analysis of amino acids. Limnol Oceanogr 62:541–560
Hunt BPV, Allain V, Menkes C, Lorrain A and others (2015) A coupled stable isotope-size spectrum approach to understanding pelagic food-web dynamics: a case study from the southwest sub-tropical Pacific. Deep Sea Res II 113:208–224
Hunt BPV, Espinasse B, Pakhomov EA, Cherel Y, Cotté C, Delegrange A, Henschke N (2021) Pelagic food web structure in high nutrient low chlorophyll (HNLC) and naturally iron fertilized waters in the Kerguelen Islands region, Southern Ocean. J Mar Syst 224:103625
Ikeda T (1985) Metabolic rates of epipelagic marine zooplankton as a function of body-mass and temperature. Mar Biol 85:1–11
Irigoien X, Klevjer TA, Rostad A, Martinez U and others (2014) Large mesopelagic fishes biomass and trophic efficiency in the open ocean. Nat Commun 5:3271
Jacob U, Mintenbeck K, Brey T, Knust R, Beyer K (2005) Stable isotope food web studies: a case for standardized sample treatment. Mar Ecol Prog Ser 287:251–253
Karl D, Letelier R, Tupas L, Dore J, Christian J, Hebel D (1997) The role of nitrogen fixation in biogeochemical cycling in the subtropical North Pacific Ocean. Nature 388:533–538
Kaunzinger CMK, Morin PJ (1998) Productivity controls food-chain properties in microbial communities. Nature 395:495–497
Kerr SR, Dickie LM (2001) The biomass spectrum: a predator-prey theory of aquatic production. Columbia University Press, New York, NY
Landry MR, Calbet A (2004) Microzooplankton production in the oceans. ICES J Mar Sci 61:501–507
Landry MR, Décima M (2017) Protistan microzooplankton and the trophic position of tuna: quantifying the trophic link between micro- and mesozooplankton in marine food webs. ICES J Mar Sci 74:1885–1892
Landry MR, Al-Mutairi H, Selph KE, Christensen S, Nunnery S (2001) Seasonal patterns of mesozooplankton abundance and biomass at Station ALOHA. Deep Sea Res II 48:2037–2061
Landry MR, Ohman MD, Goericke R, Stukel MR, Tsyrklevich K (2009) Lagrangian studies of phytoplankton growth and grazing relationships in a coastal upwelling ecosystem off Southern California. Prog Oceanogr 83: 208–216
Landry MR, Selph KE, Taylor AG, Decima M, Balch WM, Bidigare RR (2011) Phytoplankton growth, grazing and production balances in the HNLC equatorial Pacific. Deep Sea Res II 58:524–535
Landry MR, Selph KE, Décima M, Gutiérrez-Rodríguez A, Stukel MR, Taylor AG, Pasulka AL (2016) Phytoplankton production and grazing balances in the Costa Rica Dome. J Plankton Res 38:366–379
Landry MR, Stukel MR, Décima M (2020) Food-web fluxes support high rates of mesozooplankton respiration and production in the equatorial Pacific. Mar Ecol Prog Ser 652:15–32
Lavaniegos BE, Ohman MD (2003) Long-term changes in pelagic tunicates of the California Current. Deep Sea Res II 50:2473–2498
Lavaniegos BE, Ohman MD (2007) Coherence of long-term variations of zooplankton in two sectors of the California Current System. Prog Oceanogr 75:42–69
Lavaniegos BE, Molina-Gonzalez O, Murcia-Riano M (2015) Zooplankton functional groups from the California Current and climate variability during 1997–2013. CICIMAR Oceanides 30:45–62
Legendre L, Rassoulzadegan F (1995) Plankton and nutrient dynamics in marine waters. Ophelia 41:153–172
Legendre L, Rivkin RB (2008) Planktonic food webs: microbial hub approach. Mar Ecol Prog Ser 365:289–309
Li G, Cheng L, Zhu J, Trenberth KE, Mann ME, Abraham JP (2020) Increasing ocean stratification over the past half-century. Nat Clim Change 10:1116–1123
Liu KK, Kaplan IR (1989) The eastern tropical Pacific as a source of ^{15}N enriched nitrate in seawater off southern California. Limnol Oceanogr 34:820–830
Lorenzen CJ (1967) Determination of chlorophyll and pheo-pigments: spectrophotometric equations. Limnol Oceanogr 12:343–346
Macko SA, Uhle ME, Engel MH, Andrusevich V (1997) Stable nitrogen isotope analysis of amino acid enantiomers by gas chromatography combustion/isotope ratio mass spectrometry. Anal Chem 69:926–929
Marcolin CD, Schultes S, Jackson GA, Lopes RM (2013) Plankton and seston size spectra estimated by the LOPC and ZooScan in the Abrolhos Bank ecosystem (SE Atlantic). Cont Shelf Res 70:74–87
Maureaud A, Gascuel D, Colléter M, Palomares MLD, Du Pontavice H, Pauly D, Cheung WWL (2017) Global change in the trophic functioning of marine food webs. PLOS ONE 12:e0182826
McClelland JW, Montoya JP (2002) Trophic relationships and the nitrogen isotopic composition of amino acids in plankton. Ecology 83:2173–2180
McGowan JA, Walker PW (1979) Structure in the copepod community of the North Pacific Central Gyre. Ecol Monogr 49:195–226
McMahon KW, Hamady LL, Thorrold SR (2013) A review of ecogeochemistry approaches to estimating movements of marine animals. Limnol Oceanogr 58:697–714
Menden-Deuer S, Lessard EJ (2000) Carbon to volume relationships for dinoflagellates, diatoms, and other protist plankton. Limnol Oceanogr 45:569–579
Metges CC, Petzke KJ, Hennig U (1996) Gas chromatography combustion isotope ratio mass spectrometric comparison of *N*-acetyl- and *N*-pivaloyl amino acid esters to measure ^{15}N isotopic abundances in physiological samples: a pilot study on amino acid synthesis in the upper gastrointestinal tract of minipigs. J Mass Spectrom 31:367–376
Mompean C, Bode A, Benitez-Barrios VM, Dominguez-Yanes JF, Escanez J, Fraile-Nuez E (2013) Spatial patterns of plankton biomass and stable isotopes reflect the influence of the nitrogen-fixer *Trichodesmium* along the subtropical North Atlantic. J Plankton Res 35:513–525
Mompean C, Bode A, Latasa M, Fernandez-Castro B, Mourino-Carballido B, Irigoien X (2016) The influence of nitrogen inputs on biomass and trophic structure of ocean plankton: a study using biomass and stable isotope size-spectra. J Plankton Res 38:1163–1177
Ohman MD, Lavaniegos BE, Townsend AW (2009) Multidecadal variations in calcareous holozooplankton in the California Current System: thecosome pteropods, heteropods, and foraminifera. Geophys Res Lett 36:L18608
Ohman MD, Rau G, Hull P (2012) Multi-decadal variations in stable N isotopes of California Current zooplankton. Deep Sea Res I 60:46–55
Post DM (2002) Using stable isotopes to estimate trophic position: models, methods, and assumptions. Ecology 83: 703–718

Rau GH, Ohman MD, Pierrot-Bults A (2003) Linking nitrogen dynamics to climate variability off central California: a 51 year record based on $^{15}N/^{14}N$ in CalCOFI zooplankton. Deep Sea Res II 50:2431–2447

Roman MR, Dam HG, Gauzens AL, Urban-Rich J, Foley DG, Dickey TD (1995) Zooplankton variability on the equator at 140° W during the JGOFS EqPac Study. Deep Sea Res II 42:673–693

Roman MR, Dam HG, Le Borgne R, Zhang X (2002) Latitudinal comparisons of equatorial Pacific zooplankton. Deep Sea Res II 49:2695–2711

Roxy MK, Modi A, Murtugudde R, Valsala V and others (2016) A reduction in marine primary productivity driven by rapid warming over the tropical Indian Ocean. Geophys Res Lett 43:826–833

Rykaczewski RR (2019) Changes in mesozooplankton size structure along a trophic gradient in the California Current Ecosystem and implications for small pelagic fish. Mar Ecol Prog Ser 617–618:165–182

Rykaczewski RR, Checkley DM (2008) Influence of ocean winds on the pelagic ecosystem in upwelling regions. Proc Natl Acad Sci USA 105:1965–1970

Rykaczewski RR, Dunne JP (2010) Enhanced nutrient supply to the California Current Ecosystem with global warming and increased stratification in an earth system model. Geophys Res Lett 37:L21606

Ryther JH (1969) Photosynthesis and fish production in the sea. Science 166:72–76

San Martin E, Irigoien X, Harris RP, Lopez-Urrutia A, Zubkov MV, Heywood JL (2006) Variation in the transfer of energy in marine plankton along a productivity gradient in the Atlantic Ocean. Limnol Oceanogr 51:2084–2091

Schoener TW (1989) Food webs from the small to the large. Ecology 70:1559–1589

Sheridan CC, Landry MR (2004) A 9-year increasing trend in mesozooplankton biomass at the Hawaii Ocean Time-Series Station ALOHA. ICES J Mar Sci 61:457–463

Sigman DM, Karsh KL, Casciotti KL (2009) Nitrogen isotopes in the ocean. In: Steele JH (ed) Encyclopedia of ocean sciences, 2nd edn. Academic Press, Oxford, p 40–54

Steinberg DK, Lomas MW, Cope JS (2012) Long-term increase in mesozooplankton biomass in the Sargasso Sea: linkage to climate and implications for food web dynamics and biogeochemical cycling. Glob Biogeochem Cycles 26:GB1004

Stock C, Dunne J (2010) Controls on the ratio of mesozooplankton production to primary production in marine ecosystems. Deep Sea Res I 57:95–112

Stukel MR, Décima M, Landry MR, Selph KE (2018) Nitrogen and isotope flows through the Costa Rica Dome upwelling ecosystem: the crucial mesozooplankton role in export flux. Glob Biogeochem Cycles 32: 1815–1832

Taylor AG, Landry MR (2018) Phytoplankton biomass and size structure across trophic gradients in the southern California Current and adjacent ocean ecosystems. Mar Ecol Prog Ser 592:1–17

Taylor A, Landry MR, Selph KE, Yang EJ (2011) Biomass, size structure and depth distributions of the microbial community in the eastern equatorial Pacific. Deep Sea Res II 58:342–357

Taylor AG, Landry MR, Freibott A, Selph KE, Gutierrez-Rodriguez A (2016) Patterns of microbial community biomass, composition and HPLC diagnostic pigments in the Costa Rica upwelling dome. J Plankton Res 38:183–198

Ueda K, Morgan SL, Fox A, Gilbart J, Sonesson A, Larsson L, Odham G (1989) D-alanine as a chemical marker for the determination of streptococcal cell wall levels in mammalian tissues by gas chromatography negative ion chemical ionization mass spectrometry. Anal Chem 61: 265–270

Valencia B, Landry MR, Décima M, Hannides CCS (2016) Environmental drivers of mesozooplankton biomass variability in the North Pacific Subtropical Gyre. J Geophys Res Biogeosci 121:3131–3143

Valencia B, Décima M, Landry MR (2018) Environmental effects on mesozooplankton size structure and export flux at Station ALOHA, North Pacific Subtropical Gyre. Glob Biogeochem Cycles 32:289–305

Vander Zanden MJ, Rasmussen JB (2001) Variation in $\delta^{15}N$ and $\delta^{13}C$ trophic fractionation: implications for aquatic food web studies. Limnol Oceanogr 46:2061–2066

Venrick EL (2012) Phytoplankton in the California Current system off southern California: changes in a changing environment. Prog Oceanogr 104:46–58

Vinogradov ME, Shushkina EA (1978) Some development patterns of plankton communities in upwelling areas of Pacific Ocean. Mar Biol 48:357–366

Wang WL, Moore JK, Martiny AC, Primeau FW (2019) Convergent estimates of marine nitrogen fixation. Nature 566:205–211

Ward CL, McCann KS (2017) A mechanistic theory for aquatic food chain length. Nat Commun 8:2028

White JR, Zhang XS, Welling LA, Roman MR, Dam HG (1995) Latitudinal gradients in zooplankton biomass in the tropical Pacific at 140° W during the JGOFS EqPac study: effects of El Niño. Deep Sea Res II 42:715–733

Williams RL, Wakeham S, McKinney R, Wishner KF (2014) Trophic ecology and vertical patterns of carbon and nitrogen stable isotopes in zooplankton from oxygen minimum zone regions. Deep Sea Res I 90:36–47

Zhou M (2006) What determines the slope of a plankton biomass spectrum? J Plankton Res 28:437–448

Zhou M, Tande KS, Zhu YW, Basedow S (2009) Productivity, trophic levels and size spectra of zooplankton in northern Norwegian shelf regions. Deep Sea Res II 56:1934–1944

Editorial responsibility: Deborah Steinberg, Gloucester Point, Virginia, USA
Reviewed by: S. Doherty, M. Bode-Dalby and 1 anonymous referee

Submitted: September 23, 2021
Accepted: May 6, 2022
Proofs received from author(s): June 26, 2022